Article:
Rucklidge, AM orcid.org/0000-0003-2985-0976 and Postlethwaite, CM (2017) Spirals and heteroclinic cycles in a spatially extended Rock-Paper-Scissors model of cyclic dominance. EPL, 117 (4). 48006. ISSN 0295-5075

https://doi.org/10.1209/0295-5075/117/48006

Spirals and heteroclinic cycles in a spatially extended Rock–Paper–Scissors model of cyclic dominance

C. M. Postlethwaite[1] and A. M. Rucklidge[2]

[1] *Department of Mathematics, Auckland University, Auckland, NZ*
[2] *School of Mathematics, University of Leeds, Leeds LS2 9JT, UK*

PACS `47.54.Fj` – First pacs description
PACS `87.23.Cc` – Second pacs description

Abstract – Spatially extended versions of the cyclic-dominance Rock–Paper–Scissors model have traveling wave (in one dimension) and spiral (in two dimensions) behavior. The far field of the spirals behave like traveling waves, which themselves have profiles reminiscent of heteroclinic cycles. We compute numerically a nonlinear dispersion relation between the wavelength and wavespeed of the traveling waves, and, together with insight from heteroclinic bifurcation theory and further numerical results from 2D simulations, we are able to make predictions about the overall structure and stability of spiral waves in 2D cyclic dominance models.

Introduction. – Scissors cut Paper, Paper wraps Rock, Rock blunts Scissors: the simple game of Rock–Paper–Scissors provides an appealing model for cyclic dominance between competing populations or strategies in evolutionary game theory and biology. The model has been invoked to explain the repeated growth and decay of three competing strains of microbial organisms [1] and of three colour morphs of side-blotched lizards [2]. In a well-mixed population, the dynamics of the model is dominated by the presence of a heteroclinic cycle connecting the three equilibria where only one of the three species survives [3]. In continuum models, non-zero initial populations can never lead to extinction. However, in stochastic models, which include demographic fluctuations arising from the finite population size, fluctuations will lead eventually to one species becoming extinct (say Rock). When this happens, Scissors no longer has any restraint on its population and so will quickly wipe out Paper – so fluctuations lead to one of the three competitors eventually dominating [4],

When spatial distribution and mobility of species is taken in to account, waves of Rock can invade regions of Scissors, only to be invaded by Paper in turn; in a homogeous space, these waves can be organised into spirals, with roughly equal populations of the three species at the core of each spiral, and each species dominating in turn in the spiral arms [5]. Cyclic behaviour is also seen if spatial heterogeneity (patchiness) is also taken into account [6]. As such, cyclic competition with spatial structure has been invoked as a mechanism for explaining the persistence of biodiversity in nature [5,7,8], and the Rock–Paper–Scissors model with spatial structure is now an important reference model for non-hierarchical competitive relationships [1,8].

The basic processes of growth and cyclic dominance between three species can be modelled as [9]:

$$A+\phi \xrightarrow{1} A+A, \quad A+B \xrightarrow{\sigma} \phi+B, \quad A+B \xrightarrow{\zeta} B+B, \quad (1)$$

where A and B are two of the three species and ϕ represents space for growth, with growth rate 1. Species B dominates A either by removing it (at rate $\sigma \geq 0$) or by replacing it (at rate $\zeta \geq 0$). Processes for the other pairs of species are found by symmetry. Individuals are placed on a spatial lattice and allowed to move to adjacent lattice sites. Mean field equations can be derived [9,10]:

$$\begin{aligned} \dot{a} &= a(1-\rho-(\sigma+\zeta)b+\zeta c)+\nabla^2 a, \\ \dot{b} &= b(1-\rho-(\sigma+\zeta)c+\zeta a)+\nabla^2 b, \\ \dot{c} &= c(1-\rho-(\sigma+\zeta)a+\zeta b)+\nabla^2 c, \end{aligned} \quad (2)$$

where (a,b,c) are non-negative functions of space (x,y) and time t, representing the density of each of the three species, and $\rho = a+b+c$. The coefficient of the diffusion terms is set to 1 by scaling x and y, and nonlinear diffusion effects [11] are suppressed.

Without diffusion, (2) has been well studied [3]. It has five non-negative equilibria: the origin $(0,0,0)$,

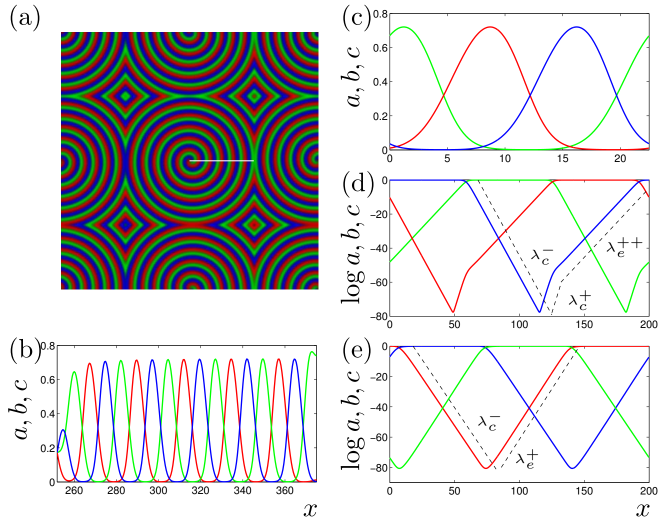

Fig. 1: Numerical solutions of equations (2), with parameters $\sigma = 3.2$, $\zeta = 0.8$ except in (d,e); a, b and c are shown in red, green and blue respectively. Panels (a) and (b) show results from integration in 2D, with domain size 500×500; the spiral waves have estimated clockwise rotation frequency $\Omega = 0.440$ and far-field wavespeed $\gamma = 1.576$ and wavelength $\Lambda = 22.5$. Panel (b) shows the profile along the white line in (a). Panels (c)–(e) show results from integrations in 1D. In (c), the box size is $\Lambda = 22.5$ (c.f. the waves in (b)). Panel (d) is for a larger box ($\Lambda = 200$), and $\zeta = 0.2$; in log coordinates a kink (change in slope) is evident in the upward phase of each curve. The estimated wavespeed is $\gamma = 1.059$. Panel (e) has $\zeta = 2$, and a profile without a kink. The estimated wavespeed is $\gamma = 2.834$. The dashed lines in (d) and (e) show slopes as indicated, labelled with eigenvalues from Table 1.

coexistence $\frac{1}{3+\sigma}(1, 1, 1)$, and three on the coordinate axes, $(1, 0, 0)$, $(0, 1, 0)$ and $(0, 0, 1)$. The origin is unstable; the coexistence point has eigenvalues -1 and $\frac{1}{2}\left(\sigma \pm i\sqrt{3}(\sigma + 2\zeta)\right)/(3 + \sigma)$, and the on-axis equilibria have eigenvalues -1, ζ and $-(\sigma + \zeta)$. When $\sigma > 0$, the coexistence point is unstable and trajectories are attracted to a heteroclinic cycle between the on-axis equilibria, approaching each in turn, staying close for progressively longer times but never stopping [3, 12, 13].

Numerical simulations of (2) in sufficiently large two-dimensional (2D) domains with periodic boundary conditions show a variety of behaviors as parameters are changed [9, 14]. Stable spiral patterns are readily found (Fig. 1a), in which regions dominated by A (red) are invaded by B (green), only to be invaded by C (blue). Comparing a cut through the core (Fig. 1b) with a one-dimensional (1D) solution with the same wavelength (Fig. 1c) demonstrates how the behavior far from the core is essentially a 1D traveling wave (TW). Stable 1D TWs can be found with arbitrarily long wavelength (Fig. 1d,e), where (apart from being periodic) the behavior closely resembles a heteroclinic cycle, with traveling fronts between regions where one variable is close to 1 and the others are close to 0.

The question we ask is: can ideas from nonlinear dynamics and heteroclinic cycles be used to analyze the properties (wavelength, wavespeed and stability) of the 1D TWs and 2D spirals? Our approach is to consider the 1D TWs as periodic orbits in a moving frame of reference, and use continuation techniques to calculate a nonlinear relationship between the wavelength and wavespeed. We find parameter ranges in which these 1D TWs exist (between a Hopf bifurcation and three different types of heteroclinic bifurcation) and obtain partial information about their stability. The locations of the heteroclinic bifurcation are computed numerically, but in two of the three cases they coincide with straight-forward relations between eigenvalues. We investigate 2D solutions of the partial differential equations (PDEs) (2) over a range of parameter values, and show numerically that the rotation frequency of the spiral is related to the imaginary part of the eigenvalues of the coexistence fixed point. Combining this information is enough to determine the overall properties of the spiral.

Analysis of traveling waves. – We first consider equations (2) in 1D, and move to a right-traveling frame moving with wavespeed $\gamma > 0$. We define $\xi = x + \gamma t$, then $\frac{\partial}{\partial x} \to \frac{\partial}{\partial \xi}$ and $\frac{\partial}{\partial t} \to \gamma\frac{\partial}{\partial \xi} + \frac{\partial}{\partial t}$. Traveling wave solutions in the moving frame have $\frac{\partial}{\partial t} = 0$, and so TW solutions of (2) correspond to periodic solutions of the following set of six first-order ODEs:

$$
\begin{aligned}
a_\xi &= u, & u_\xi &= \gamma u - a(1 - \rho - (\sigma + \zeta)b + \zeta c), \\
b_\xi &= v, & v_\xi &= \gamma v - b(1 - \rho - (\sigma + \zeta)c + \zeta a), \\
c_\xi &= w, & w_\xi &= \gamma w - c(1 - \rho - (\sigma + \zeta)a + \zeta b).
\end{aligned} \tag{3}
$$

The period (in ξ) of the periodic solution corresponds to the wavelength Λ of the TW, and in numerical simulations of the PDEs in 1D with periodic boundary conditions, the size of the computational box.

Let $\boldsymbol{x} = (a, u, b, v, c, w)$. The coexistence and on-axis equilibria of the ODEs (3) are $\boldsymbol{x} = \frac{1}{3+\sigma}(1, 0, 1, 0, 1, 0)$, $(1, 0, 0, 0, 0, 0)$, $(0, 0, 1, 0, 0, 0)$ and $(0, 0, 0, 0, 1, 0)$. We label these equilibria ξ_h, ξ_a, ξ_b and ξ_c respectively. The eigenvalues of the equilibrium ξ_a are given in table 1. By symmetry, ξ_b and ξ_c have the same eigenvalues. It can easily be seen that the four-dimensional subspace $\{c = w = 0\}$ is invariant under the flow of (3). Restricted to this subspace, ξ_a has a three-dimensional unstable manifold, and ξ_b has a two-dimensional stable manifold, which generically intersect, and there is thus a robust heteroclinic connection between ξ_a and ξ_b. By symmetry, we have a robust heteroclinic cycle between ξ_a, ξ_b and ξ_c.

Following conventions used in the analysis of heteroclinic cycles (see e.g. [13]) we label the eigenvalues as radial, contracting and expanding (see again table 1). For ξ_a, the radial eigenvectors lie in the subspace $\{b = v = c = w = 0\}$, the contracting eigenvectors in the subspace $\{b = v = 0\}$ and the expanding eigenvectors in the subspace $\{c = w = 0\}$. Note that this labelling does not exactly correspond with the definitions given in [13] and

Table 1: Eigenvalues of the on-axis equilibria of (3). The radial and contracting eigenvalues are always real, and satisfy $\lambda_r^- < 0 < \lambda_r^+$ and $\lambda_c^- < 0 < \lambda_c^+$. If $\gamma^2 > 4\zeta$, the expanding eigenvalues are also real, and $\lambda_e^{++} > \lambda_e^+ > 0$. If $\gamma^2 < 4\zeta$, the expanding eigenvalues $\lambda_e^R \pm i\lambda_e^I$ are complex, and $\lambda_e^R > 0$.

Label	Eigenvalues
Radial	$\lambda_r^\pm = \frac{1}{2}\left(\gamma \pm \sqrt{\gamma^2+4}\right)$
Contracting	$\lambda_c^\pm = \frac{1}{2}\left(\gamma \pm \sqrt{\gamma^2+4(\sigma+\zeta)}\right)$
Expanding ($\gamma^2 - 4\zeta > 0$)	$\lambda_e^{++}_{+} = \frac{1}{2}\left(\gamma \pm \sqrt{\gamma^2-4\zeta}\right)$
Expanding ($\gamma^2 - 4\zeta < 0$)	$\lambda_e^R \pm i\lambda_e^I = \frac{1}{2}\left(\gamma \pm i\sqrt{4\zeta-\gamma^2}\right)$

other similar papers, mostly because of the presence of a positive contracting eigenvalue, which means that the unstable manifold of the equilibrium is not contained in the 'expanding' subspace. However, we find the labelling useful because the eigenvalues play similar roles as to those seen in the literature, even though they do not exactly fit the definitions.

In numerical solutions of the PDEs (2) in large 1D periodic domains of size Λ, these infinite-period heteroclinic cycles are excluded and we find instead periodic solutions that lie close to the heteroclinic cycle. These solutions spend a lot of "time" (a large interval in the ξ variable) close to the equilibria, where the components grow (or decay) exponentially with rates equal to the relevant eigenvalues (see Fig. 1d,e). In large domains the TW profiles are thus determined by their wavelength Λ and these eigenvalues. We find large-Λ TWs with three different profiles; two of which are shown in Fig. 1(d,e). The kinked profile in (d) takes the form:

$$\log a(\xi) = \begin{cases} 0 & 0 \le \xi \le \frac{\Lambda}{3} \\ \lambda_c^-\left(\xi - \frac{\Lambda}{3}\right) & \frac{\Lambda}{3} < \xi \le \frac{\Lambda}{3} + l \\ \lambda_c^- l + \lambda_c^+\left(\xi - \frac{\Lambda}{3} - l\right) & \frac{\Lambda}{3} + l < \xi \le \frac{2\Lambda}{3} \\ \log a\left(\frac{2\Lambda}{3}\right) + \lambda_e^{++}\left(\xi - \frac{2\Lambda}{3}\right) & \frac{2\Lambda}{3} < \xi \le \Lambda \end{cases}$$

and b and c are cyclic permutations, so $b(\xi) = a(\xi + \frac{\Lambda}{3})$ and $c(\xi) = b(\xi + \frac{\Lambda}{3})$. The amount of "decay" in the contracting phase must match the amount of growth in the expanding phase, and these are both of equal length. In this case, this means there is a switch from decay to growth during the contracting phase at $\xi = \frac{\Lambda}{3} + l$, where $l = \frac{\Lambda}{3}\frac{\lambda_c^+ + \lambda_e^{++}}{\lambda_c^+ - \lambda_c^-}$ (and $0 < l < \frac{\Lambda}{3}$), and a change in the upwards slope (a kink) at $\xi = \frac{2\Lambda}{3}$. The solution is continuous, periodic and $\log a(\Lambda) = 0$. We have ignored the "time" taken for jumps between the equilibria (which round the sharp corners of the profile) as these are short compared to Λ, so long as Λ is sufficiently large. Generically, when the expanding eigenvalues are real, we expect solutions leaving a neighbourhood of an equilibrium to do so tangent to the leading

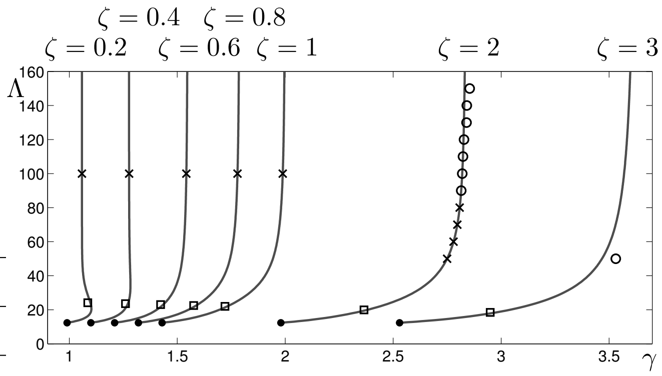

Fig. 2: The wavelength (period in ξ) Λ, as γ is varied, of periodic orbits in the ODEs (3), computed using AUTO, with $\sigma = 3.2$ and values of ζ as indicated. Each curve of periodic orbits arises in a Hopf bifurcation on the left (black dot), and ends in a heteroclinic (long-period) bifurcation on the right. Effectively these curves are nonlinear dispersion relations for TWs in the PDEs. Symbols indicate the results of 1D TW and 2D spiral solutions of the PDEs (2), as described in the text.

expanding eigenvector: i.e. with an expansion rate equal to λ_e^+. The profile observed in Fig. 1(d) is non-generic, and corresponds to an orbit flip, discussed further later. The profile in Fig. 1(e) has no kink, and the rate of expansion is λ_e^+ rather than λ_e^{++}. The third profile observed is similar to that in Fig. 1(d) except the expanding eigenvalues are very slightly complex.

Although the heteroclinic cycle exists robustly in the ODEs, periodic solutions cannot be found by forward integration since they are not stable with respect to evolution in the ξ variable. Instead, we identify a Hopf bifurcation at the equilibrium ξ_h, and use the continuation software AUTO [15] to follow periodic orbits, treating the wavespeed γ as a parameter, allowing the wavelength Λ to be adjusted automatically.

The Jacobian matrix at ξ_h has pure imaginary eigenvalues $\pm i\omega_H$ when $\gamma = \gamma_H(\sigma, \zeta)$, where

$$\gamma_H(\sigma,\zeta) \equiv \frac{\sqrt{3}(\sigma+2\zeta)}{\sqrt{2\sigma(\sigma+3)}}, \quad \text{and} \quad \omega_H^2 = \frac{\sigma}{2(\sigma+3)}, \qquad (4)$$

at which point a Hopf bifurcation creates periodic orbits of period $\Lambda_H = \frac{2\pi}{\omega_H}$. Fig. 2 shows, for $\sigma = 3.2$ and a range of values of ζ, the wavelength (period in ξ) Λ as γ is varied. The range of γ for which periodic solutions can be found depends on σ and ζ; each branch starts at γ_H and terminates with infinite Λ in a heteroclinic bifurcation.

In Fig. 3 we show a bifurcation diagram of the ODEs (3) (computed by AUTO) in (γ, ζ) space. The red and blue curves correspond to simple equalities of the eigenvalues, as indicated in the figure, and divide the parameter space into four labelled regions, defined in table 2. Periodic solutions bifurcate to the right of the Hopf bifurcation, given by (4), into region 3 (except for very small ζ) and

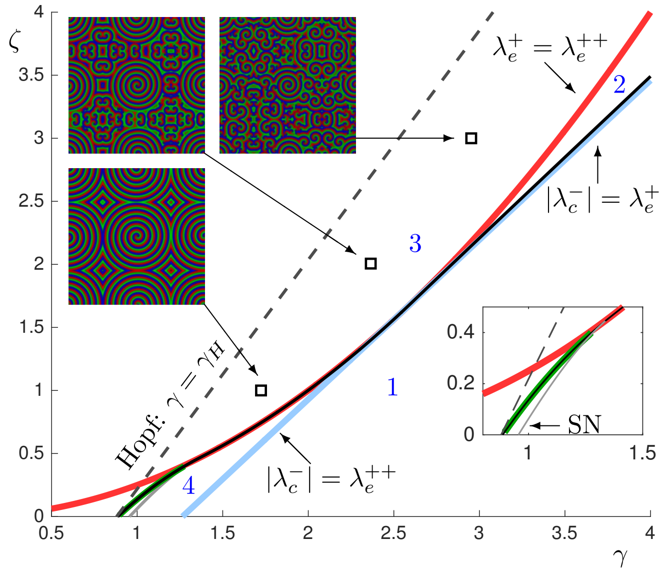

Fig. 3: Bifurcation diagram for the ODEs (3), in (γ, ζ) parameter space, with $\sigma = 3.2$. The blue line ($\zeta = \sqrt{\frac{\sigma}{2}}\gamma - \frac{\sigma}{2}$) and red curve ($4\zeta = \gamma^2$) are tangent at $(\gamma, \zeta) = (\sqrt{2\sigma}, \sigma/2)$ and divide the parameter space into four regions, labeled by blue numbers, and defined in table 2. The green curve is the locus of a heteroclinic orbit flip. The dark grey dashed line is a curve of Hopf bifurcations. Periodic orbits bifurcate to the right of this line and disappear in a curve of heteroclinic bifurcations (black). A curve of saddle-node bifurcations of periodic orbits (light grey) exists for smaller ζ. The upper insets show 2D simulations at the indicated parameter values. The lower inset is a zoom near the saddle-node (SN) and orbit flip (green) bifurcations.

disappear in the heteroclinic bifurcation curve (black) on the right. In 1D PDE simulations, this corresponds to observing small wavelength travelling waves just after the Hopf bifurcation (in region 3) which grow in wavelength as γ increases and disappear at the black curve. Note that the dynamics for the PDEs (2) and the ODEs (3) only coincide when the travelling wave solutions exist, i.e. betwen the Hopf curve (dashed line) and the heteroclinic curve (black curve).

We observe from the numerical results that the heteroclinic bifurcation in Fig. 3 shows three different behaviors, overlying the green, red and blue curves in different parameter regimes, corresponding to the three large-Λ TW profiles discussed earlier. Note that heteroclinic bifurcations cannot occur in the interiors of regions 2 or 3. In region 2, a large-Λ TW profile would require $l > \frac{\Lambda}{3}$, which cannot occur. In region 3, the expanding eigenvalues are complex. In the large Λ limit, complex eigenvalues are excluded: the invariance of the subspace $\{a = u = 0\}$ means that a cannot change sign along trajectories.

When $\zeta > \frac{\sigma}{2} = 1.6$, the heteroclinic bifurcation occurs on the blue curve, along which the negative contracting and leading expanding eigenvalues are equal in magnitude, and the TW has an unkinked profile (Fig. 1(e)). This is a heteroclinic resonance bifurcation [16]. For $0.4 < \zeta < \frac{\sigma}{2} = 1.6$, the heteroclinic bifurcation occurs on the red curve, along which the expanding eigenvalues switch from complex to real (a variant of a Belyakov–Devaney bifurcation [17]), and the TW has a kinked profile. For $0 < \zeta < 0.4$, the periodic orbit undergoes a saddle-node bifurcation before the heteroclinic bifurcation; the fold can be seen in the curve for $\zeta = 0.2$ in Fig. 2. Here, the heteroclinic bifurcation coincides with an orbit flip bifurcation [18], indicated in green in Fig. 3. The TW has a kinked profile, as in Fig. 1(d). The location of the orbit flip is computed by solving a boundary value problem in the four-dimensional invariant subspace $\{c = w = 0\}$ that requires that the heteroclinic solutions is tangent to the λ_e^{++} eigenvector.

Returning to the PDEs (2), we computed solutions over a range of values of σ, ζ and domain size. We imposed periodic boundary conditions, and used fast Fourier transforms and second-order exponential time differencing [19]. In 2D, we mainly used 1000×1000 domains, with 1536 Fourier modes in each direction. We estimated speeds of TWs (in 1D) and rotation frequencies and far-field wavelengths and wavespeeds of spirals (in 2D).

In 1D, with $\sigma = 3.2$ and $\zeta < \frac{\sigma}{2} = 1.6$, we are able to find stable TWs for all box sizes larger than Λ_H. For $\zeta > \frac{\sigma}{2}$, we find that TWs are stable in smaller boxes, and unstable in larger boxes, with a decreasing range of stable boxes sizes as ζ is increased. For $\zeta = 3$, we are unable to find any stable TWs. The crosses (resp. open circles) in Fig. 2 show the observed wavespeeds of stable (resp. unstable) TWs for a range of ζ and box sizes. In this context, by "stable" we are referring to how the TWs evolves in time with a fixed wavelength. A full treatment of stabiliity would include convective and absolute instability of the TWs.

In 2D, spiral waves (or more complex solutions) are usually found if the domain is large enough. We use initial conditions that are one half a and a quarter each b and c, as in [11]. When we find spirals, we locate the core (where $a = b = c$) and compute the far-field wavelength by taking a cut through the core (Fig. 1(a,b)). The angular frequency Ω is obtained from a timeseries (the temporal period is $2\pi/\Omega$), and the wavespeed is $\gamma = \Lambda\Omega/2\pi$. For $\sigma = 3.2$ and a selection of ζ, we have included in Fig. 3 three examples, along with their (γ, ζ) values, and in Fig. 2 (as open squares) the (γ, Λ) values estimated from spiral solutions. The fact that the open square symbols lie on the continuation curves from AUTO confirms that the far field of the spirals obeys the same nonlinear dispersion relation as 1D solutions.

We now have two relations between three quantities, the rotation frequency Ω of the 2D spiral, and the wavespeed γ and wavelength Λ of the 1D TWs in the far field. When locating the core we observed that the common value of the three variables is almost $\frac{1}{3+\sigma}$, the value from the coexistence equilibrium. We therefore compared the rotation frequency Ω to the imaginary part of the complex eigenvalue at the coexistence equilibrium, plotting (in Fig. 4)

Table 2: Definitions of the regions of parameter space shown in Fig. 3 and eigenvalue properties therein.

Region	Definition	Eigenvalue properties
1	$\zeta < \sqrt{\frac{\sigma}{2}}\gamma - \frac{\sigma}{2}$	$\lambda_e^{++} \in \mathbb{R}$, $\lambda_e^{+} < \lvert\lambda_c^{-}\rvert < \lambda_e^{++}$
2	$\zeta > \frac{\sigma}{2}$, $\sqrt{\frac{\sigma}{2}}\gamma - \frac{\sigma}{2} < \zeta < \frac{\gamma^2}{4}$	$\lambda_e^{++} \in \mathbb{R}$, $\lvert\lambda_c^{-}\rvert < \lambda_e^{+} < \lambda_e^{++}$
3	$\zeta > \frac{\gamma^2}{4}$	$\lambda_e^{++} \in \mathbb{C}$
4	$\zeta < \frac{\sigma}{2}$, $\sqrt{\frac{\sigma}{2}}\gamma - \frac{\sigma}{2} < \zeta < \frac{\gamma^2}{4}$	$\lambda_e^{++} \in \mathbb{R}$, $\lambda_e^{+} < \lambda_e^{++} < \lvert\lambda_c^{-}\rvert$

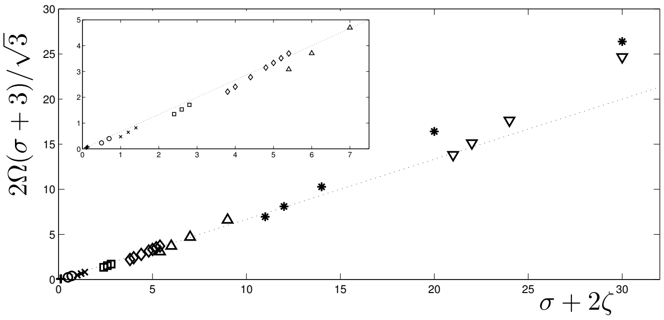

Fig. 4: The scaled spiral frequency $2\Omega(\sigma+3)/\sqrt{3}$ plotted against $\sigma+2\zeta$, for results from 2D simulations over a range of σ and ζ. The dotted line has a slope of $\frac{2}{3}$. The inset shows a zoom of the origin. Different symbols correspond to different values of σ: $(0.1, 0.5, 1, 2, 3.2, 5, 10, 20) = (+, \bigcirc, \times, \square, \lozenge, \triangle, \star, \triangledown)$.

$\frac{2}{\sqrt{3}}\Omega(\sigma+3)$ against $\sigma+2\zeta$. The data almost collapses on to a straight line of slope (approximately) $\frac{2}{3}$, over the range of σ and ζ that we investigated. If Ω were *equal* to the imaginary part of the complex eigenvalue, the slope would be 1. For each value of σ, indicated by the symbols in Fig. 4, the value "$\frac{2}{3}$" depends weakly on ζ, with increasing departure from this value for larger σ.

This data collapse is sufficient to give a complete prediction for the properties of a spiral: the angular frequency Ω is set by the core and is approximately $\frac{2}{3}\frac{\sqrt{3}}{2}(\sigma+2\zeta)/(3+\sigma)$. The other two quantities γ and Λ are set by $\gamma = \Lambda\Omega/2\pi$ and the nonlinear dispersion relation in Fig. 2.

It remains to consider the far-field stability of the spirals. As can be seen in the insets in figure 3, the size of the spirals in the 2D simulations appears to decrease as ζ is increased. With $\sigma = 3.2$, we find 1000×1000 domain-filling 2D spirals (as in Fig. 1a) over the range $0.2 \leq \zeta \leq 1.2$. For values of ζ outside this range, the far field of the spiral breaks up, and for $\zeta = 0.2$ and $\zeta \geq 1.1$, this is also seen in a larger domains. This pattern is repeated with other values of σ: in the range $0.1 \leq \sigma \leq 20$, we find stable domain-filling spirals in a finite range of ζ; for small σ and ζ, the wavelengths of the spirals are so big that only a few turns fit in to the domain. The spiral wavelengths are typically about $2\Lambda_H$, which suggests from (4) that for small σ the wavelength scales as $\sigma^{-\frac{1}{2}}$. The same scaling can be deduced from the results (based on a completely different approach) of [10]

Discussion. – Models related to (2) with one species ($b = c = 0$, the Fisher–KPP equation) and with two species ($c = 0$, the Lotka–Volterra system) are used to describe moving fronts between regions of different genes or species. Although in these models the equilibria having real eigenvalues imposes a constraint on the wavespeed, the speed that is observed is set by details of the initial population profiles. In the case of the Fisher–KPP equation, there is a lower bound of 2 on the front propagation speed [20]. Our success in describing the dynamics of spirals in the three-species case, without reference to details of the initial conditions, relies on the interesting structures being periodic TW, rather than fronts, and on these TW arising in a Hopf bifurcation, which is absent in the Fisher–KPP equantion and the Lotka–Volterra system.

Our approach complements that taken by [7], where spirals are described in terms of a Complex Ginzburg–Landau equation (CGLE). Strictly, this description requires a Hopf bifurcation from the coexistence equilibrium in (2). There is a (degenerate) Hopf bifurcation at $\sigma = 0$. Its degeneracy can be broken by including the effect of mutation [21], and an asymptotic description of small-amplitude (weakly nonlinear) spirals close to the coexistence equilibrium can be inferred by reducing (2) (with mutation) to the CGLE [10,11]. In contrast, our approach treats the TW as fully nonlinear, close to a heteroclinic cycle. The stability predictions cannot be compared directly, and true 2D spirals are in between these two extremes, but both approaches yield a $\sigma^{-\frac{1}{2}}$ scaling (for small σ) of the wavelength of the TWs.

In spite of the prevalence of spirals in this model, spirals have yet to be observed in nature or in experiments involving non-hierarchical competitive relationships between species. It may be that the model is too simple and neglects important effects [22, 23], it may be that the system is operating in a regime where spirals are entirely fragmented (and indeed the parameters are hard to estimate [24]), or it may be that the spirals that should be present are in fact larger than the domain under consideration or smaller than the spacing between sampling locations [25]. Notwithstanding these caveats, the Rock–Paper–Scissors model remains an appealing reference model for cyclic competition.

* * *

The authors would like to thank Graham Donovan, Edgar Knobloch, Mauro Mobilia and Hinke Osinga for helpful discussions regarding this work. This work was started during a visit of CMP to Leeds partly funded by a Scheme 2 grant from the London Mathematical Society and the University of Auckland.

REFERENCES

[1] Kerr B., Riley M. A., Feldman M. W. and Bohannan B. J. M., *Nature*, **418** (2002) 171.
[2] Sinervo B. and Lively C. M., *Nature*, **380** (1996) 240.
[3] May R. M. and Leonard W. J., *SIAM J. Appl. Math*, **29** (1975) 243.
[4] Kerr B., Neuhauser C., Bohannan B. J. M. and Dean A. M., *Nature*, **442** (2006) 75.
[5] Reichenbach T., Mobilia M. and Frey E., *Nature*, **448** (2007) 1046.
[6] Schreiber S. J. and Killingback T. P., *Theoretical population biology*, **86** (2013) 1.
[7] Reichenbach T., Mobilia M. and Frey E., *J. Theor. Biol.*, **254** (2008) 368.
[8] Szolnoki A., Mobilia M., Jiang L., Szczesny B., Rucklidge A. M. and Perc M., *J. Roy. Soc. Interface*, **11** (2014) 20140735.
[9] Frey E., *Physica A*, **389** (2010) 4265.
[10] Szczesny B., Mobilia M. and Rucklidge A. M., *Phys. Rev. E*, **90** (2014) 032704.
[11] Szczesny B., Mobilia M. and Rucklidge A. M., *EPL*, **102** (2013) 28012.
[12] Guckenheimer J. and Holmes P., *Math. Proc. Camb. Phil. Soc.*, **103** (1988) 189.
[13] Krupa M. and Melbourne I., *Ergod. Theory Dyn. Syst.*, **15** (1995) 121.
[14] Orihashi K. and Aizawa Y., *Physica D*, **240** (2011) 1853.
[15] Doedel E. J., Paffenroth R. C., Champneys A. R., Fairgrieve T. F., Kuznetsov Y. A., Sandstede B. and Wang X., Tech. Rep. Caltech (2001).
[16] Scheel A. and Chossat P., *C. R. Acad. Sci. Paris Ser. I*, **314** (1992) 49.
[17] Champneys A. R., *Physica D*, **112** (1998) 158.
[18] Homburg A. J. and Krauskopf B., *Journal of Dynamics and Differential Equations*, **12** (2000) 807.
[19] Cox S. M. and Matthews P. C., *J. Comp. Phys.*, **176** (2002) 430.
[20] FISHER R. A., *Ann. Eugenics*, **7** (1937) 355.
[21] Mobilia M., *J. Theor. Biol.*, **264** (2010) 1.
[22] Weber M. F., Poxleitner G., Hebisch E., Frey E. and Opitz M., *J. Roy. Soc. Interface*, **11** (2014) 2014017.
[23] Kelsic E. D., Zhao J., Vetsigian K. and Kishony R., *Nature*, **521** (2015) 516.
[24] Warne D. J., Baker R. E. and Simpson M. J., , (2016) .
[25] Mobilia M., Rucklidge A. M. and Szczesny B., *Games*, **7** (2016) 24.